Hard Superellipse Phases: Particle Shape Anisotropy & Curvature

Isaac Torres-Díaz,[†‡] *Rachel S. Hendley,*[†] *Akhilesh Mishra, Alex J. Yeh, and Michael A. Bevan**
Chemical & Biomolecular Engineering, Johns Hopkins University, Baltimore, MD 21218

Abstract

We report computer simulations of two-dimensional convex hard superellipse particle phases vs. particle shape parameters including aspect ratio, corner curvature, and sidewall curvature. Shapes investigated include disks, ellipses, squares, rectangles, and rhombuses, as well as, shapes with non-uniform curvature including rounded squares, rounded rectangles, and rounded rhombuses. Using measures of orientational order, order parameters, and a novel stretched bond orientational order parameter, we systematically identify particle shape properties that determine liquid crystal and crystalline phases including their coarse boundaries and symmetry. We observe phases including isotropic, nematic, tetratic, plastic crystals, square crystals, and hexagonal crystals (including stretched variants). Our results catalog known benchmark shapes, but include new shapes that also interpolate between known shapes. Our results indicate design rules for particle shapes that determine two-dimensional liquid, liquid crystalline, and crystalline microstructures that can be realized via particle assembly.

Introduction

Assembling anisotropic particles into microstructured materials is important for understanding and designing particle based materials with complex emergent properties useful for diverse applications.[1-4] For example, different shaped particles can be assembled to mimic natural periodic materials with novel multifunctional properties.[2,3] In reviews of anisotropic particles,[1-6] a broad variety of particle shapes are cataloged including natural and synthetic materials (*e.g.*, clays, viruses, metal, metal oxide, and polymer colloids, etc.) that are too expansive to review here. Typical shapes often include platelets, rods, ellipsoids, superellipsoids, polyhedra, as well as increasingly complex shapes that defy a single consistent taxonomy.[1] Such particles form layers on solid and fluid interfaces, and often monolayers, which are useful for surface coatings with complex optical, mechanical, electrical, acoustic, wetting, adhesive, and other properties. In such cases, understanding the two-dimensional phase behavior of different anisotropic particle shapes is important to designing and controlling assembled microstructures.

Two-dimensional hard particle phase behavior has received significant attention in theory and simulations. For the simplest case of hard disks, the phase diagram has been shown to have liquid, hexatic, and crystal phases, where the hexatic phase has quasi-long range six-fold bond orientational order and short-range positional order.[7-12] Introducing anisotropy by stretching hard disks into hard ellipses also produces liquid and crystalline phases, as well as, liquid crystalline phases with two-fold orientational order referred to as a nematic phase.[13,14] Low aspect ratio hard ellipses also have plastic crystal phases, which have positional order but not orientational order.[15] Corners on hard squares[16] and hard rectangles[17,18] produce tetratic phases intermediate to liquids and crystals, which have quasi-long range four-fold orientational order and short-range positional

†These authors contributed equally to this work.
‡Current address: Chemical & Materials Engr., Univ. of Alabama, Huntsville, AL 35899
*To whom correspondence should be addressed: mabevan@jhu.edu

order. Studies of hard squares continuously rounded to hard disks illustrate how different liquid crystal and crystal microstructures vary as corner curvature changes.[19,20] Many other two-dimensional hard shapes have been studied (*e.g.*, polygons,[21] unique shapes[22]) too numerous to summarize here.

The cited modeling studies, and numerous experimental studies, have carefully investigated hard two-dimensional shapes to identify phases, phase boundaries, transition order, equations of state, etc. However, we are not aware of a systematic study of hard particle phase behavior for both continuously varying aspect ratio and curvature. Anisotropic particle curvature can lead to different liquid crystal phases such as nematic phases in hard ellipses,[13] tetratic phases in hard rectangles,[17,22] and smectic phases in three dimensional spherocylinders.[23] Unintended curvature is often present in experiments due to particle fabrication limitations, which can produce significant effects in experimentally observed phase behavior.[24-28] In addition, realistic colloidal potentials generally include short-range soft repulsion and/or attraction, which can often be considered as effective hard particles with perturbation theories.[29] However, such realistic interactions can vary at particle corners and edges (*e.g.*, platelets,[30] quasi-2d rods[31]) in a manner that could be treated as effective corner curvature. Many open questions remain about how particle aspect ratio and curvature together determine phase behavior and order.

In this work, we systematically investigate hard superellipse phases and their coarse boundaries using Monte Carlo (MC) simulations. The surface of a superellipse is represented by,[32]

$$\left|x/r_x\right|^n + \left|y/r_y\right|^n = 1 \tag{1}$$

where r_x and r_y are the particle semi-axes, aspect ratio is r_y/r_x, and n defines particle shape. As shown in **Fig. 1**, superellipse shapes include disks (n=2, r_y/r_x=1), ellipses (n=2, r_y/r_x<1), squares ($n\to\infty$, r_y/r_x=1), and rectangles ($n\to\infty$, r_y/r_x<1), which we use as benchmarks for validation and to catalog superellipse phase behavior. Curvature of the superellipse surface is given by,

$$\gamma = \frac{(n-1)\left|x\right|^{n-2}\left|y\right|^{n-2}}{r_x^n r_y^n \left(\frac{\left|x\right|^{2n-2}}{r_x^{2n}} + \frac{\left|y\right|^{2n-2}}{r_y^{2n}}\right)^{3/2}} \tag{2}$$

which can be used to systematically quantify and define sidewall and corner curvature for each shape (**Fig. 1**, *e.g.*, to $\gamma r_x \gtrsim 3$ and sidewalls have $\gamma r_x \lesssim 0.3$). Superellipses include previously unstudied shapes (*e.g.*, rhombuses) and provide a well-defined way to continuously vary aspect ratio and corner and sidewall curvature to investigate their combined effects on positional and orientational order in different phases. We are unaware of a comprehensive summary of phases for hard superellipses. Our study focuses on hard superellipse phases for the shapes in **Fig. 1** (including more aspect ratios). We also develop novel stretched bond orientational order parameters to quantify order in superellipse phases. Our goal is to understand how curvature and aspect ratio together determine different types of phases, their approximate boundaries, and their positional and orientational order. Our results are intended to provide a basis to understand and design two dimensional microstructures of different shaped particles on solid and fluid interfaces in numerous applications.

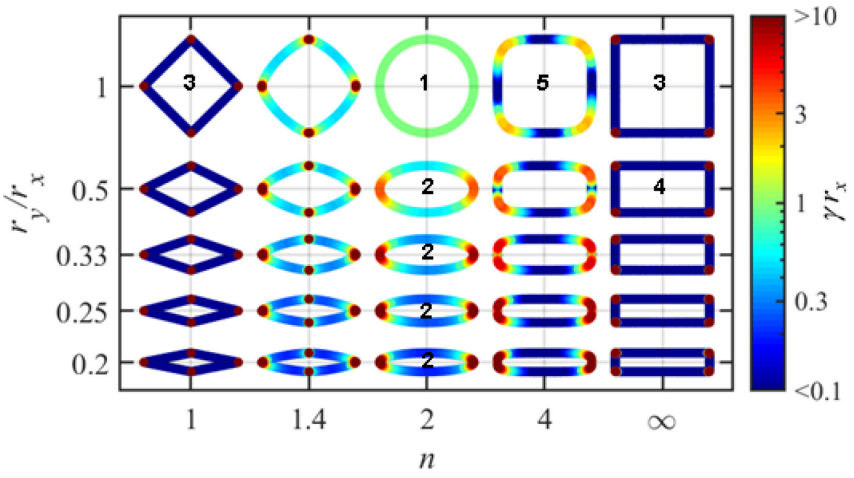

Fig. 1. Superellipse shapes vs. aspect ratio r_y/r_x and the parameter n (Eq. (1)). The outline of each shape is colored to depict the local curvature (Eq. (2)), where corner features can be considered to correspond to $\gamma r_x \gtrsim 3$ and sidewalls have $\gamma r_x \lesssim 0.3$. Previously studied benchmark cases include: (**1**) disks (n=2, r_y/r_x=1),[7-12] (**2**) ellipses (n=2, r_y/r_x<1),[13,15] (**3**) squares ($n\to\infty$, r_y/r_x=1),[16] (**4**) rectangles ($n\to\infty$, r_y/r_x<1),[17,18] and (**5**) rounded squares (n≈3-10, r_y/r_x=1).[19,20]

Methods

Computer Simulations

Computer simulations were implemented using a standard MC algorithm in the NVT ensemble, similar to prior two-dimensional hard particle studies.[14,17,21] We do not use the NPT ensemble or compute pressure[11,33,34] since we do not attempt to obtain equations of state. We simulated two-dimensional systems of uniform superellipses defined by Eq. (1) with different aspect ratios and shapes (**Fig. 1**). Simulations in a square simulation box with periodic boundary conditions were used to obtain all area fractions by melting from the maximum packed configuration for each shape (Λ_0 crystal structure).[35] Simulations were equilibrated for $>10^6$ steps before quantifying orientational order and order parameters, which are averaged over $\sim 10^4$ independent configurations.

Simulations were performed for N≈700-1000 hard particles. For each shape, the number of particles was increased from 700 until the pair correlation function spans >25 particle radii to ensure a sufficient range for correlation functions. System sizes of N≈700-1000 were chosen based on prior studies of system size dependent hard particle phase behavior for different shapes contained within the superellipse shape class. MC simulations of hard ellipses with N>400 are sufficient for obtaining accurate phase diagrams.[14,15] MC simulations of rounded hard squares, ranging from disks to squares, with N=400 capture phases and boundaries on the order of $0.01\,\eta$, as validated by simulations of much larger system sizes for hard disks (N=1024^2),[12] hard squares (N=1024^2),[21] and hard superdisks (N=6400).[20] Likewise, MC simulations of hard rectangles[17,18] for N=10^3-10^4 suggest larger system sizes are required to resolve phase boundaries on the order of $0.01\,\eta$. Exceptionally large system sizes of N=1024^2 particles have been used to resolve all aspects of hexatic transitions of hard disks[12] and tetratic transitions of hard squares.[21] Based on this precedent, N>700 is sufficient for our goals of resolving phases with approximate boundaries without a detailed analysis of phase transitions. Finally, as will be shown in our results, our MC simulations with N≈700-1000 capture all phases and coarse boundaries for key hard particle

benchmark shapes, including: hard disks,[12] hard ellipses,[14] hard squares,[21] hard rectangles,[17] and hard rounded squares.[20] We revisit discussions of system size effects in the context of our findings.

Hard Superellipse Overlap

Overlap between superellipses is determined using three levels of approximation. The first estimate is based on separation between centers of circles circumscribing each particle. No overlap is guaranteed if the center-to-center distance is greater than the diameter of the circumscribed circle. If this condition is not satisfied, a second estimate is based on circumscribing rectangles around each superellipse particle and determining minimum distances between superellipses to x and y planes of circumscribed rectangles (see *Supporting Information* (*SI*) **Fig. S1**) as,

$$h_x = \left(|x| - r_x\right) - \left[\left|r_x A_{11}\right|^{\frac{n}{n-1}} + \left|r_y A_{21}\right|^{\frac{n}{n-1}}\right]^{\frac{n-1}{n}}$$
$$h_y = \left(|y| - r_y\right) - \left[\left|r_x A_{12}\right|^{\frac{n}{n-1}} + \left|r_y A_{22}\right|^{\frac{n}{n-1}}\right]^{\frac{n-1}{n}} \quad (3)$$

where $|x|$ and $|y|$ are vector components between particle centers, r_x, and r_y are superellipse semi-axes, A_{ij} is the component of the relative rotation transformation matrix between the two particles.[36,37] Eq. (3) must be applied for both particles in a pair, and if one value of h_x or h_y, is positive, it guarantees no overlaps. If the first two conditions are not satisfied, a final estimate employs a refined mesh to evaluate the superellipse function $f(x,y) = |x/r_x|^n + |y/r_y|^n - 1$ for every point on the second particle; $f(x,y)>0$ guarantees no-overlaps.

Bond Orientational Order

To measure the local symmetry of particles relative to neighbor particles, a novel stretched local bond orientational order parameter is defined as,

$$\psi_{n,j} = \frac{1}{N_{b,j}}\left|\sum_{k=1}^{N_{b,j}} \exp\left(in\theta_{jk}\right)\right| = \frac{1}{N_{b,j}}\left|\sum_{k=1}^{N_{b,j}} \cos\left(n\theta_{jk}\right) + i\sin\left(n\theta_{jk}\right)\right| \quad (4)$$

where $N_{b,j}$ is the number of neighbors with bonds to particle j, and θ_{jk} is the angle between particle centers relative to an arbitrary axis. To implement Eq. (4) for anisotropic particles, it is necessary to identify neighbors and account for particle shape, which we briefly describe in the following.

First, we describe neighbor determination. Although four-fold (n=4) order is commonly calculated for hard squares based on the four closest neighbors,[19] and six-fold (n=6) order is calculated for hard disks, rounded squares, and regular polyhedra based on all neighbors,[7-9,21] tessellation schemes have been suggested as a more robust approach to neighbor determination.[38] For anisotropic particles with different aspect ratios and curvatures, accurate identification of neighbors in concentrated conditions requires tessellation based on surfaces (rather than particle centers).[39,40] In our work, the tessellated space is calculated along the continuous path connecting the locus of centers of circles tangent to the surface of different shaped particles (red lines **Fig. S2a,c**, tessellated space for many particles **Fig. S2b,d**).

Next, we consider particle symmetry in the calculation of stretched four-fold $\psi_{4,j}$ and six-fold $\psi_{6,j}$ bond orientational order parameters (Eq. (4), illustrative shapes in **Fig. 2**). As particles become anisotropic, the usual bond orientational order does not capture structural transitions.

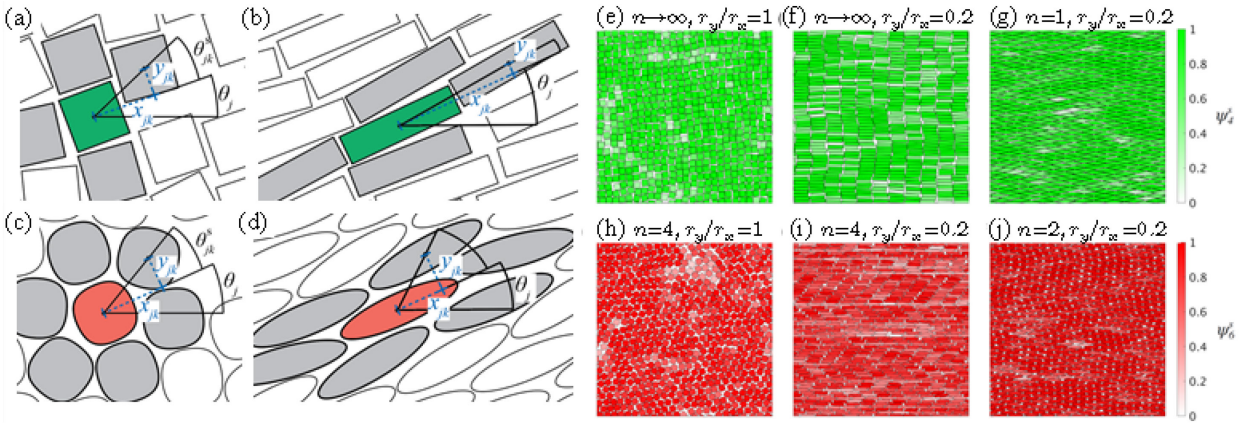

Fig. 2. Neighbor identification and stretched bond orientational order. (**left**) (top) In the case of $\psi_{4,j}$, illustration for (a) squares (n=∞, r_y/r_x=1) and (b) rectangles (n=∞, r_y/r_x=0.2), around central particle (green) and 4 neighbors (grey) by relative center position x_{jk} and y_{jk} (blue). (bottom) In the case of $\psi_{6,j}$, illustration for (c) rounded squares (n=4, r_y/r_x=1) and (d) ellipses (n=2, r_y/r_x=0.25) around central particle (red). (**right**) Various particle configurations colored by local stretched bond orientation order parameters (Eq. (4)) for (e-g) 4-fold order and (h-j) 6-fold order with shape parameters labelled on figures.

Since the interval of neighboring particle angles changes for $r_y/r_x \neq 1$, we adapt the usual bond orientational order parameter for anisotropic particles by defining θ_{jk} in Eq. (4) as,

$$\theta_{jk} = \theta_{jk}^{s} + \theta_{j} \tag{5}$$

where θ_j is the angle between the main axis of the particle and the reference axis (**Fig. 2**), and θ_{jk}^{s} is the neighbor angle in a stretched coordinate system given by,

$$\cos\theta_{jk}^{s} = x_{jk}/r_e\,,\quad \sin\theta_{jk}^{s} = y_{jk}/r_e\,,\quad r_e = \sqrt{\left(x_{jk}/r_x\right)^2 + \left(y_{jk}/r_y\right)^2} \tag{6}$$

where the x_{jk} and y_{jk} are the relative components of the neighbor's position with respect to the principle axis of the particle of interest. Also, r_e is the center-to-center distance between the two particles in the stretched coordinate system. Eq. (6) also yields $\theta_{jk}^{s} = \tan^{-1}[(y_{jk}/r_y)/(x_{jk}/r_x)]$. Practically, the local bond orientational order for anisotropic particles (Eq. (4)) is determined via a stretching transformation of nearest neighbor coordinates that effectively corresponds to a unity aspect ratio about the central particle. The stretched local bond orientational order in Eq. (4) can also be adapted to compute the stretched global bond orientational order as,

$$\psi_n = \left|\frac{1}{N_b}\sum_j\sum_k \exp\left(in\theta_{jk}\right)\right| = \left|\frac{1}{N_b}\sum_j\sum_k \cos\left(n\theta_{jk}\right) + i\sin\left(n\theta_{jk}\right)\right| \tag{7}$$

where N_b is the total number of bonds in the system.

Correlation Functions & Order Parameters

Phases are determined from the long-range power-law decay of orientational order correlation functions. For isotropic particles, the correlation function for bond orientational order of order m is given as,[7-9,19,21]

$$g_m(\mathbf{r}) = \left\langle \psi_{m,j}(\mathbf{r})\psi_{m,k}^{*}(\mathbf{r}')\right\rangle \tag{8}$$

and for anisotropic particles, a particle orientational correlation function of order m is given by,[17,41,42]

$$G_m(r) = \left\langle \cos\left[m\left(\theta_{jk}(r) - \theta_j\right)\right]\right\rangle \tag{9}$$

where θ_{jk} is the angle between particle pair centers relative to a fixed arbitrary axis. Both Eqs. (8) and (9) exhibit a long-range power-law decay as,

$$g_m(r) \sim r^{\kappa_m}, \; G_m(r) \sim r^{\kappa_m} \tag{10}$$

where fitting κ_m is used to develop criteria for the presence of phases with long-range order. For example, $|\kappa_m| < 0.25$ has been used to identify the liquid-hexatic transition for hard disks[7,8] and isotropic-nematic transition for anisotropic particles.[41,42] Likewise, $|\kappa_m| < 0.5$ has been used to identify the liquid- tetratic transition for hard squares[16,19] and rectangles.[17]

Nematic and tetratic order parameters indicate how well particles are oriented along the director or bidirector of a particle configuration. The nematic order parameter is calculated from the second-order nematic tensor, [41]

$$\mathbf{S}_{ij} = \left\langle 2n_i n_j - \delta_{ij} \right\rangle \tag{11}$$

as the positive eigenvalues, S_2. The nematic order parameter can alternatively and equivalently be calculated by maximizing the average over each particles orientation relative to the nematic director as, $S_2=\max\langle\cos[2(\theta_j-\theta_2)]\rangle$, where θ_2 is the nematic director. The tetratic order parameter is calculated from the unfolded fourth-order tetratic matrix,[16,17,43]

$$\mathbf{T}_{ijkl} = \left\langle 4n_i n_j n_k n_l - \frac{1}{2}\left(\delta_{ij}\delta_{kl} + \delta_{ik}\delta_{jl} + \delta_{il}\delta_{jk}\right)\right\rangle \tag{12}$$

as the eigenvalues $(0, -T_4, 0.5[T_4 - (16S_2 + T_4^2)^{0.5}], 0.5[T_4 + (16S_2 + T_4^2)^{0.5}])$. The tetratic order parameter can also be calculated by maximizing the average over each particles orientation relative to the bidirector as, $T_4=\max\langle\cos[4(\theta_j-\theta_4)]\rangle$, where θ_4 is the bidirector angle. The smectic order parameter is,[44]

$$\sigma = \max_d \left\langle \cos\left(2\pi r_{\theta_2}/d\right)\left(2\cos\theta_2 - 1\right)\right\rangle \tag{13}$$

which measures particle positions relative to the nematic director, θ_2, by maximizing S_2,[44,45] and layering with period, d, obtained by maximizing σ. Positions, $r_{\theta 2}$, are measured for each particle along the nematic director.

Phase Determination

We briefly describe phase determination as captured concisely in **Figs. S4-5, Tables S1-2**. Threshold values for the long range power law decay of orientational correlation functions, κ_m (Eq. (10)) determine the presence of liquid crystal and crystal phase with m-fold order using the inequalities in **Table S1** and flow chart in **Fig. S4** (illustrative examples in **Fig. S3**). However, construction of orientational correlation functions requires significant statistics from temporal, spatial, and ensemble sampling,[11,12] which make them less practical for determining phases for combinations of small, non-uniform, and dynamic systems.[46-48] Based on this consideration, we also list how order parameters alone (Eqs. (4), (11)-(13)) can be used to estimate phases with

threshold inequalities (**Table S2, Fig. S5**) that yield boundaries in agreement with the results from orientational correlation functions. These criteria for phase determination agree with prior benchmark cases for hard disks,[7-10] hard ellipses,[13,15] hard squares,[16] rounded hard squares,[19,20] and hard rectangles[17,18] with similar system sizes. Based on this agreement, the order parameter based criteria can be used in future studies (*e.g.*, microscopy experiments) involving small, non-uniform, and dynamic systems of hard superellipse particles.)

Results & Discussion

We systematically investigate hard superellipse phases for the shapes depicted in **Fig. 1**, including a total of 40 shapes and the specified benchmark cases. As will be shown, our results agree with benchmarks, which provides a foundation to explore how different combinations of aspect ratio and roundedness of corners together determine phases of more diverse shapes (while being anchored to well-established limiting cases). We note that we don't aim to resolve phase boundaries or coexistence regions to high resolution for any single shape; but rather, our goal is to comprehensively map phases and microstructure for a single hard shape class to understand systematic variations in aspect ratio and rounded corners. We leave for future studies resolving phase boundaries, coexistence, transition order, equations of state, etc. for single particle shapes where such details are of particular interest.

In the following, for values of the shape parameter, n (**Fig. 1**), we report: (1) for a single aspect ratio of $r_y/r_x = 0.2$, detailed plots of order parameters and orientational correlation function decay values vs. area fraction (η), and (2) a phase diagram in the ranges of $r_y/r_x = 0.2$-1 and $\eta = 0.4$-η_{max}. Particle shape is defined in terms of anisotropy via aspect ratio (r_y/r_x) and corner and sidewall curvature (Eq. (2), **Fig. 1**) via the superellipse parameter (n). For n=2, superellipses reduce to ellipses including isotropic disks. For $1<n<2$, intermediate values between the rhombus (n=1) and the ellipse (n=2) yields shapes with curved sidewalls joining at corners with curvature $\rightarrow \infty$ as $n \rightarrow 1$. For $n>2$, sidewalls become flatter and corner curvature increases $\rightarrow \infty$ as $n \rightarrow \infty$. Results are organized for increasing n including: rhombuses (n=1), rounded rhombuses (n=1.4), ellipses (n=2), rounded rectangles (n=4), and rectangles (n=∞).

Rhombuses (*n=1*)

Superellipses with n=1 correspond to rhombuses including squares for r_y/r_x=1. Focusing first on the highest aspect ratio investigated (r_y/r_x=0.2, **Fig. 3**), the long-range power-law decay of orientational order (κ_2, κ_4, κ_6) shows an isotropic-nematic transition near $\eta \approx 0.45$ and a nematic-crystal transition near $\eta \approx 0.78$. These transition concentrations show good correspondence to those determined from nematic and tetratic order parameters (S_2, T_4). The crystal has long-range 4-fold orientational order (κ_4) and stretched 4-fold bond orientational order (ψ_4^s). Experiments on 2D assembly of rhombus micro- and nano- particles with rounded corners,[25] and possibly concave sidewalls,[28] have rhombic crystal structures matching the configuration described by the stretched four-fold symmetry (ψ_4^s). Such experiments involve different interactions due to spherical depletants and surface ligands, but show correspondence to our results for similar shapes.

An interesting aspect of the anisotropic rhombus behavior is that stretched 4-fold bond orientational order emerges continuously in the nematic phase for $\eta>0.6$ and approaches $\psi_4^s \approx 0.5$ at concentrations just below crystallization (before $\kappa_4>0.99$). The tetratic and nematic order parameters approach unity in the same concentration range, although $S_2 > T_4$ at all concentrations. All of this together indicates the emergence of simultaneous long-range 2-fold and 4-fold

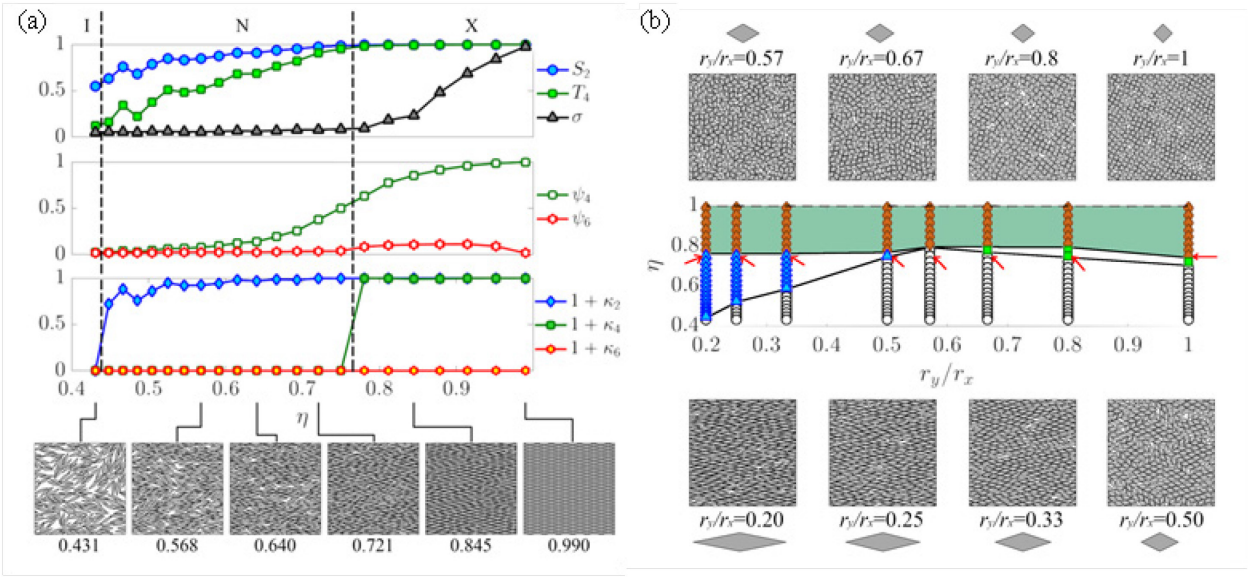

Fig 3. For rhombuses (superellipses with n=1), (**a**) and for r_y/r_x=0.2, as a function of area fraction (η), (*top*) nematic, S_2, tetratic, T_4, and smectic, σ, order parameters, (*middle*) symmetry via stretched four-fold (ψ_4^s) and six-fold (ψ_6^s) parameters, and (*bottom*) orientational order correlation function decay values (κ_2, κ_4, κ_6). Phases indicated as: (I) isotropic, (N) nematic, and (X) crystal, with symmetry indicated as (4F) four-fold. (**b**) Phase diagram vs. r_y/r_x and η with phases (from **Fig. S6**) indicated as: (○) isotropic, (▲) nematic, (■) tetratic, or (◆) crystal, with symmetry indicated as (■) four-fold. Panels show characteristic configurations at (left) indicated particle concentrations, and (right) red arrows.

orientational order along with significant 4-fold bond orientational order – all at concentrations just below where crystallization occurs. This may suggest the possibility of a tetratic phase for more anisotropic rhombuses in larger systems sizes, similar to nearly isotropic rhombuses.

We now investigate how phases depend on rhombus aspect ratio including the hard square limit (r_y/r_x =1). The complete concentration dependent order parameters, bond orientational orders, and orientational correlation decay values for r_y/r_x=0.25-1 are reported in **Fig. S6**, and the resulting phases vs. r_y/r_x and η is summarized in **Fig. 3**. Several clear trends are observed. The crystal has 4-fold order in all cases, and intermediate to liquid and crystal phases, aspect ratios from r_y/r_x≈0.57-1 have a tetratic phase whereas aspect ratios from r_y/r_x =0.2-0.57 have a nematic phase. At r_y/r_x≈0.57, there does not appear to be a liquid crystal phase. For r_y/r_x=1, our findings are in agreement with prior literature for hard squares[16,21,49] within the limits of resolution of our data. Experiments on squares involve some rounding of corners,[24,26,50] which has been shown to produce plastic crystals rather than tetratic phases.[18,19] This motivates understanding how rounded sidewalls (n<2) and corners (n>2) influence anisotropic particle phases in the following sections.

Rounded Rhombuses (n=1.4)

Superellipses with n=1.4 correspond to rounded rhombuses, where the sidewalls are curved rather than the corners (*i.e.*, nonzero convex sidewall curvature, infinite corner curvature). Starting with the highest aspect ratio (r_y/r_x=0.2) rounded rhombus, results show isotropic, nematic, and crystal phases not unlike the regular rhombus of the same aspect ratio. Although significant long range 4-fold orientational order emerges within the nematic phase, it is always less than long range 2-fold orientational order. In contrast to regular rhombuses, both stretched 4-fold and 6-fold bond orientational order emerge within the nematic and are of comparable magnitudes, although 6-fold bond orientational order is greater at concentrations just below the crystal phase. The crystal also

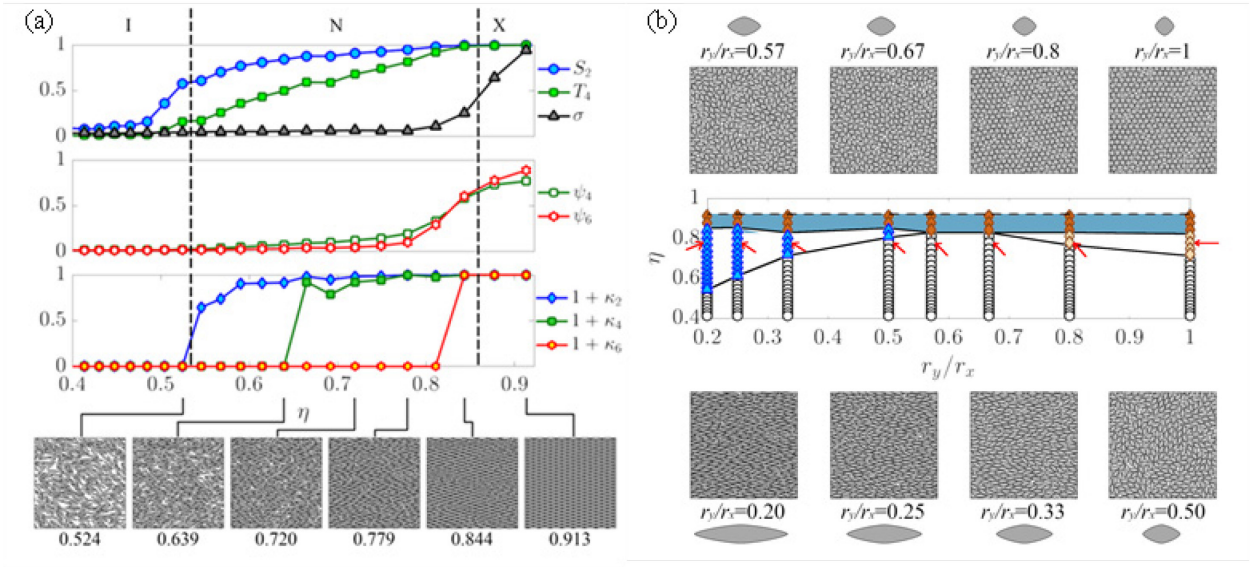

Fig. 4 For rounded rhombuses (superellipses with n=1.4), (**a**) and for r_y/r_x=0.2, as a function of area fraction (η), (*top*) nematic, S_2, tetratic, T_4, and smectic, σ, order parameters, (*middle*) symmetry via stretched four-fold (ψ_4^s) and six-fold (ψ_6^s) parameters, and (*bottom*) orientational order correlation function decay values (κ_2, κ_4, κ_6). Phases indicated as: (I) isotropic, (N) nematic, or (X) crystal, with symmetry indicated as (6F) six-fold. (**b**) Phase diagram vs. r_y/r_x and η with phases (from **Fig. S7**) indicated as: (○) isotropic, (△) nematic, (◇) plastic crystal, or (◆) crystal, with symmetry indicated as (■) six-fold. Panels show characteristic configurations at (left) indicated particle concentrations, and (right) red arrows.

has stretched long range 6-fold orientational and bond orientational order.

The results for all rounded rhombus aspect ratios considered in the analysis are in the supplementary information (**Fig. 4**, details for other r_y/r_x in **Fig. S7**). When crystals of rounded rhombuses with relatively small anisotropy ($r_y/r_x > 0.7$) melt, 6-fold bond orientational order remains high while all order parameters for particle orientational order vanish (*i.e.*, S_2, T_4, σ), indicating a plastic crystal phase. In contrast, for increasingly anisotropic rounded rhombuses ($r_y/r_x < 0.5$), a nematic phase is observed with both stretched 4-fold and 6-fold bond orientational order at concentrations just below the crystal boundary. Intermediate aspect ratio rounded rhombuses have neither plastic nor nematic phases intermediate to liquid and crystal phases.

The rounded rhombus results (**Fig. 4**) show several trends due to the effects of curved sidewalls compared to the flat sidewalls of regular rhombuses (**Fig. 3**). Although the most anisotropic rhombus and rounded rhombus share the same phases with a shift to higher concentration and narrower ranges, the rounded rhombuses show 6-fold order in the nematic and crystal phases in contrast to the 4-fold order in the nematic and crystal phases for regular rhombuses. With decreasing anisotropy, 6-fold ordered crystals are observed for all rounded rhombuses while 4-fold crystals are observed for all regular rhombuses. A clear difference due to the sidewall curvature of the rounded and regular rhombuses for less anisotropic particles is the presence of a plastic crystals instead of a tetratic phase intermediate to liquid and crystal phases. Experiments on attractive squares[24] and nearly isotropic rhombuses[25] with rounded corners both have plastic crystal phases similar to rhombuses with rounded sidewalls, but have crystal with the same symmetry as regular rhombuses.

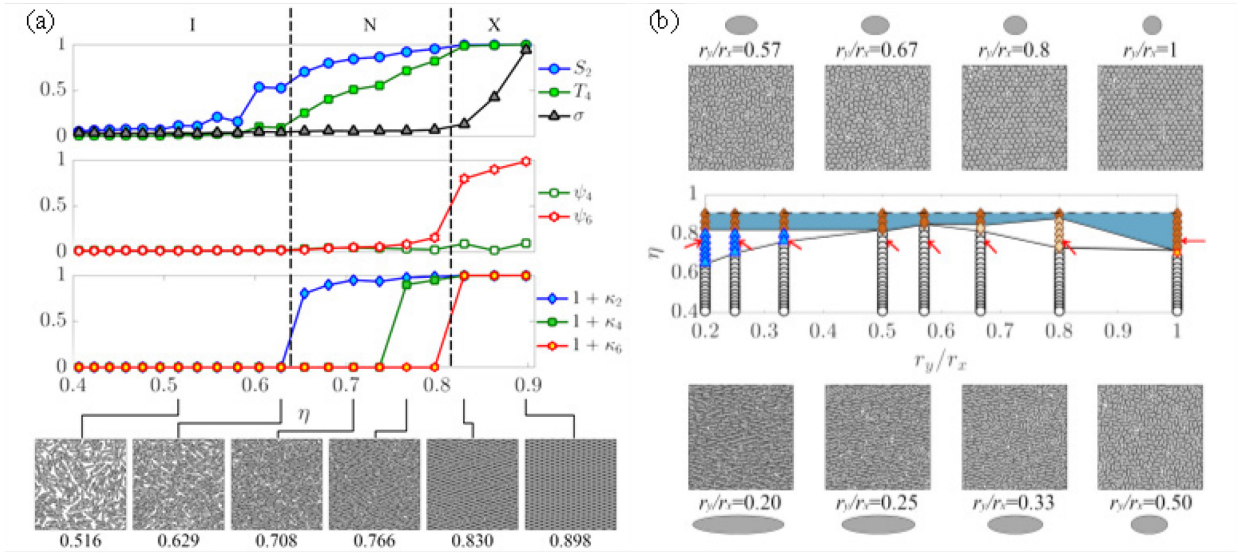

Fig. 5. For ellipses (superellipses with n=2), (**a**) and for r_y/r_x=0.2, as a function of area fraction (η), (*top*) nematic, S_2, tetratic, T_4, and smectic, σ, order parameters, (*middle*) symmetry via stretched four-fold (ψ_4^s) and six-fold (ψ_6^s) parameters, and (*botto m*) orientational order correlation function decay values (κ_2, κ_4, κ_6). Phases indicated as: (I) isotropic, (N) nematic, or (X) crystal. (**b**) Phase diagram vs. r_y/r_x and η with phases (from **Fig. S8**) indicated as: (○) isotropic, (△) nematic, (◇) plastic crystal, or (◆) crystal, with symmetry indicated as (■) six-fold. Hexatic phase (✸) from large system size literature results.[11,12] Panels show characteristic configurations at (left) indicated particle concentrations, and (right) red arrows.

Ellipses (n=2)

Hard ellipses (n=2) have been widely studied as a function of aspect ratio[13-15] including the important limiting case of hard disks.[7-12] The phase boundaries, transition order, equations of state, and mechanisms for transitions of hard disks have been determined to high precision using a number of simulation methods and exceptionally large system sizes.[11,12] Compared to all other superellipse shapes, the ellipse has finite continuous curvature around its perimeter without sharp corners or flat sidewalls. As such, hard disk and hard ellipse results provide an important benchmark for the other shapes investigated in this work.

Detailed concentration dependent order parameters, long-range orientational order, and bond orientational order are shown for ellipses with r_y/r_x=0.2 as well as phases for ellipses with r_y/r_x=0.2-1 (**Fig. 5**, details for other r_y/r_x in **Fig. S8**). As expected, for more anisotropic ellipses (r_y/r_x <0.4), long-range orientational order indicates transitions from isotropic to nematic to crystal phases at concentrations in agreement with prior studies.[13,15] Likewise, for more isotropic ellipses (r_y/r_x >0.67), a plastic crystal phase is observed intermediate to isotropic and crystal phases without observation of a nematic phase. The plastic crystal has long-range 6-fold orientational and bond orientational order but no significant preferential alignment of particles along a director. For a narrow range of aspect ratios ($0.4 < r_y/r_x < 0.67$), isotropic and crystal phases are not separated by an intermediate phase, as expected.[13-15] Signatures of both nematic ordering and plastic crystallinity are observed in this range, but are below critical thresholds, and are likely a system size effect.[41] We also note here that we do not resolve the hexatic phase and its boundaries based on its strong system size dependence, although we mark its expected location (**Fig. 5**),[11,12] which indeed is found between the liquid and crystal phases for our hard disk results.

When comparing ellipses to other shapes with corners investigated thus far, several

contrasting behaviors are observed. The most anisotropic ellipses show the same isotropic, nematic, and crystal phases as rhombuses and rounded rhombus particles with phase boundaries shifted to a narrower range at higher concentrations as sidewall curvature increases and corner curvature decreases. In addition, there is no observation of either stretched 4-fold or 6-fold bond orientational order in the ellipse nematic phases at concentrations just below crystallization. The least anisotropic ellipses have a plastic crystal phase similar to rounded rhombuses, but neither display the tetratic phase observed for nearly isotropic rhombuses (and squares); finite curvature in either sidewalls or corners seems to suppress tetratic order. The plastic crystal concentration range appears expanded for ellipses compared to rounded rhombuses presumable as the result of more moderate curvature and absence of sidewalls or corners. The crystal phase has 6-fold order similar to rounded rhombuses (n=1.4) but different from the 4-fold order for rhombuses (n=1), so clearly corners influence crystalline packing and the presence of plastic crystal phases.

Rounded Rectangles (n=4)

Superellipses with n=4 correspond to rounded rectangles, where the corners are curved rather than the sidewalls (*i.e.*, zero sidewall curvature, finite corner curvature). This contrasts rounded rhombuses where (n=1.4) where the corners are sharp and the sidewalls are curved. Again, considering the highest aspect ratio (r_y/r_x=0.2) case first for n=4 (**Fig. 6**), it has isotropic, nematic, and crystal phases. Similar to rhombuses with the same aspect ratio (n=1, **Fig. 3**), the n=4 crystal has 4-fold symmetry at low densities and also displays continuous emergence of stretched 4-fold bond orientational order in the nematic phase prior to the onset of crystallization. The highest density crystal has 6-fold order since we start all simulations from the Λ_0 configuration, which has been shown as the highest density crystal for n=4 superellipses with r_y/r_x=1 (*i.e.*, superdisks).[35] The concentration range for each phase is much narrower and occurs at higher concentrations for

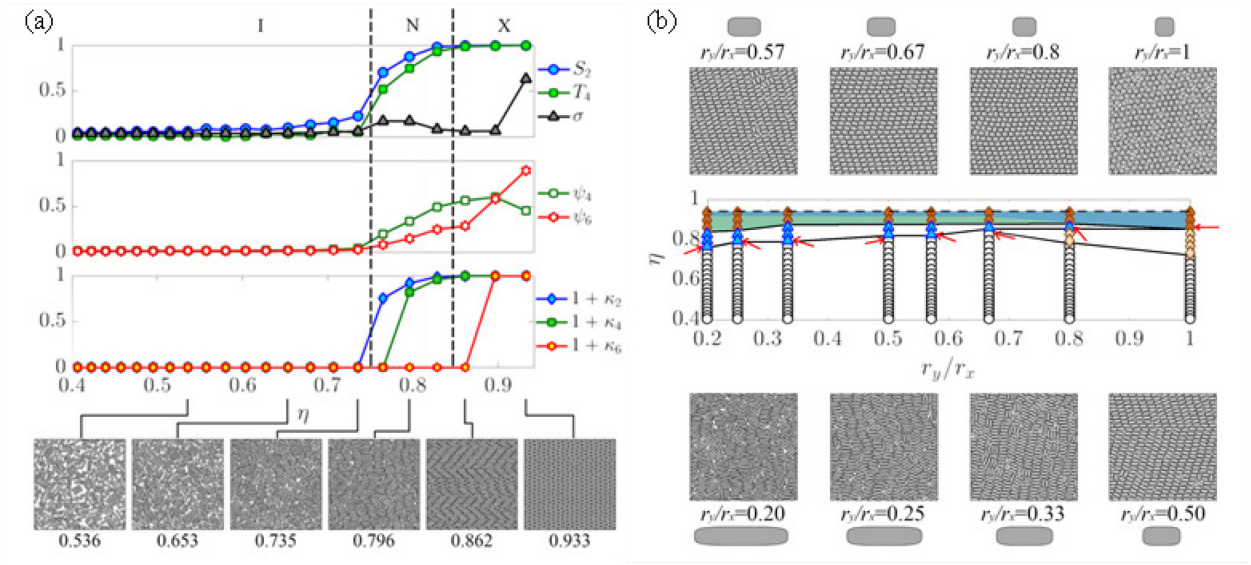

Fig. 6. For rounded rectangles (superellipses with n=4), (**a**) and for r_y/r_x=0.2, as a function of area fraction (η), (*top*) nematic, S_2, tetratic, T_4, and smectic, σ, order parameters, (*middle*) symmetry via stretched four-fold (ψ_4^s) and six-fold (ψ_6^s) parameters, and (*bottom*) orientational order correlation function decay values (κ_2, κ_4, κ_6). Phases indicated as: (I) isotropic, (N) nematic, or (X) crystal, with symmetry indicated as (4F) four-fold. (**b**) Phase diagram vs. r_y/r_x and η with phases (from **Fig. S9**) indicated as: (○) isotropic, (△) nematic, (◇) plastic crystal, or (◆) crystal, with symmetry indicated as (■) four-fold or (■) six-fold. Panels show configurations at (left) indicated particle concentrations, and (right) red arrows.

n=4 vs. n=1, so rounded rectangles have clear quantitative differences compared to rhombuses.

Another important shape within rounded rectangles (n=4) is rounded squares. The limit of rounded squares have been the subject of significant prior investigation[18,19] and provides another important benchmark. For both superdisks[20] and similar models for rounded corners with constant curvature,[19] the phase types and boundaries agree within the precision of our results (*e.g.*, compared to n=4 in Ref.[20] and $\zeta \approx 0.67$ case in Ref.[19]). Practically, the rounded hard squares in this work show a plastic crystal phase intermediate to an isotropic phase and a crystal phase. The crystal phase has long range 4-fold orientational order and relatively high 6-fold and 4-fold bond orientational order. The crystal phase is consistent with the rhombic crystal phase carefully characterized in Ref.[19] (as a result, we do not make further effort to characterize the crystal phase in this work, but refer readers to this prior study). Once again, the highest density state is the Λ_0 configuration for n=4 superdisks.[35] Quasi two-dimensional experiments with rounded square platelets[24] and rounded cubes,[26,27] each with different corner curvatures, but approximately in the vicinity of $n \approx 4$, also show primarily rhombic lattices, which correlates with our findings. However, each of these experiments also involve varying degrees of depletion attraction and soft electrostatic repulsion, which in some case is also observed to result in square lattices.

Between the highest and lowest aspect ratio rounded rectangles, the n=4 superellipse has interesting behavior at intermediate aspect ratios (**Fig. 6**, details for other r_y/r_x in **Fig. S9**). As with rounded rhombuses and ellipses, the rounded rectangles have plastic phases for less anisotropic particles ($r_y/r_x \gtrsim 0.8$) and nematic phases for more anisotropic particles ($r_y/r_x \lesssim 0.8$). Both nematic and plastic phases are observed in the vicinity of $r_y/r_x \approx 0.8$, which contrasts all other shapes in this work with more rounded corners and sidewalls (but not rectangles with sharper corners in **Fig. 7**). Also, in contrast to other shapes in this study, the nematic and plastic phase concentration ranges are the narrowest for rounded rectangles, although the reason for this is not obvious. Another observation is that flatter sidewalls on rounded rectangles produce nematic phases in less anisotropic aspect ratios than ellipses and rounded rhombuses.

All aspect ratios investigated display similar behavior in the crystal phase in terms of having both high 6-fold and 4-fold bond orientational order. For low density crystals, there is a trend of more 6-fold bond orientational order for crystals of more isotropic aspect ratio particles that transitions into more 4-fold bond orientational order for crystals of more anisotropic aspect ratio particles. These results suggest the flat sidewalls of anisotropic rounded rectangle (n=4) particles promotes stretched four-fold symmetry, perhaps similar to anisotropic regular rhombus (n=1) particles. And once again, all of the highest density crystals have 6-fold order since we start all simulations from the Λ_0 configuration.[35]

Rectangle ($n \to \infty$)

For superellipses with n tending towards infinity, the shape is a rectangle or square where sidewalls have zero curvature and corners have infinite curvature (**Fig. 7**, details for other r_y/r_x in **Fig. S10**). This shape class has received significant attention for the limiting case of squares[16,19,21] and different aspect ratio rectangles treated at varying levels of approximation.[17,18] Again, considering the highest aspect ratio (r_y/r_x=0.2) case first for $n \to \infty$ (**Fig. 7**), it displays isotropic, nematic, and crystal phases. The crystal phase had four-fold order similar to rhombuses and rounded rectangles. The onset of nematic order occurs at lower concentrations than rounded rectangles of the same aspect ratio, although the concentration is higher than the rest of the shapes investigated in this work. Also similar to all other shapes in this work, except the ellipse, 4-fold

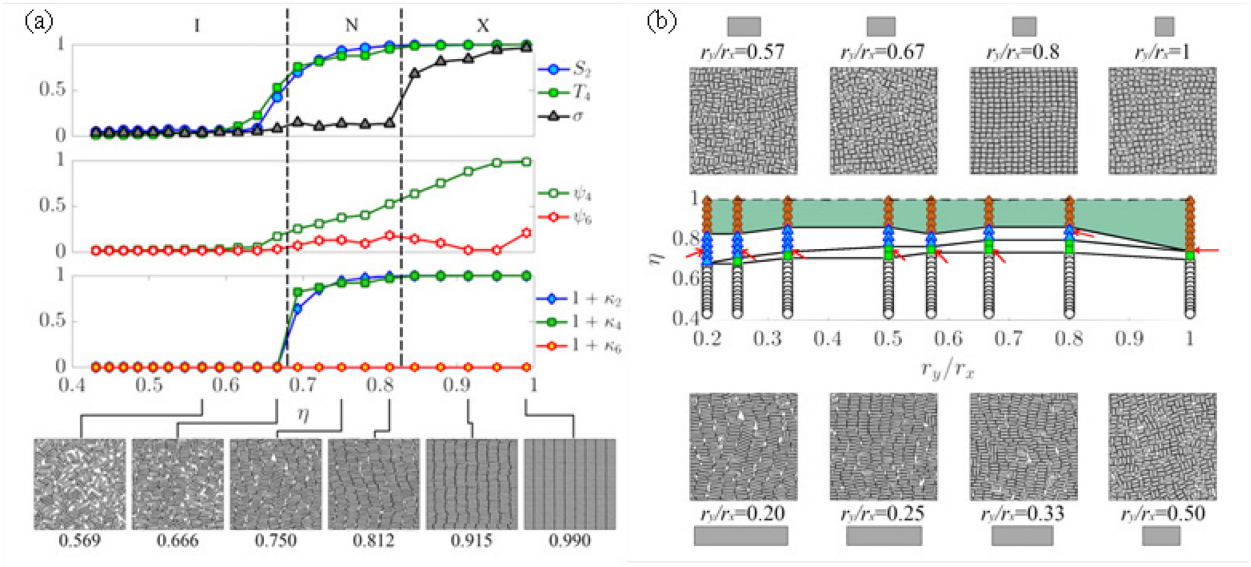

Fig. 7. For rectangles (superellipses with n=∞), (**a**) and for r_y/r_x=0.2, as a function of area fraction (η), (*top*) nematic, S_2, tetratic, T_4, and smectic, σ, order parameters, (*middle*) symmetry via stretched four-fold (ψ_4^s) and six-fold (ψ_6^s) parameters, and (*bottom*) orientational order correlation function decay values (κ_2, κ_4, κ_6). Phases indicated as: (I) isotropic, (N) nematic, or (X) crystal, with symmetry indicated as (4F) four-fold. (**b**) Phase diagram vs. r_y/r_x and η with phases (from **Fig. S12**) indicated as: (O) isotropic, (△) nematic, (■) tetratic, or (◆) crystal, with symmetry indicated as (■) four-fold. Panels show characteristic configurations at (left) indicated particle concentrations, and (right) red arrows.

bond orientational order emerges continuously in the nematic phase up to the onset of crystallization of a crystal phase of the same symmetry.

The highest aspect ratio case does not show a tetratic phase (r_y/r_x=0.2, **Fig. 7**), but all other lower aspect ratio hard rectangles and squares do show a tetratic phase (**Fig. S10**). The occurrence of the tetratic phase in hard squares is known,[16,21] and our results (**Fig. S10a**) agree with the expected lower concentration (η≈0.7) for the onset of the tetratic phase, although the range is known to depend strongly on system size.[19,21] For intermediate aspect ratios (r_y/r_x=0.25-0.8), we observe isotropic, tetratic, nematic, and crystal phases in this order. The nematic phases in these cases also have a high tetratic order parameter and four fold order. This trend smoothly varies between the limits of no nematic phase for squares, and no tetratic phase for r_y/r_x=0.2 rectangles. Rectangles formed by square dimers (*i.e.*, r_y/r_x=0.5) have also shown a tetratic phase at the same concentration as this work (η≈0.7, within the limits of uncertainty due to system size effects).[17] An approximate theory has also shown qualitatively similar results to ours in **Fig. 7** for isotropic-tetratic-nematic transitions for aspect ratios in the range r_y/r_x=0.25-0.8 and only a nematic phase for higher aspect ratios (r_y/r_x<0.25).[18,43] The trend of isotropic-tetratic-nematic transitions appears unique to rectangles with sharp corners as it is not observed in rounded rectangles. We are not aware of experiments on rectangular particles with sharp corners, including quasi-2D cylindrical particles with rectangular cross-sections.

Overview of Hard Superellipse Phases

The results for discrete values of the superellipse parameter, n in Eq. (1), show how systematically varying sidewall and corner curvature determine phase boundaries vs. concentration and aspect ratio (**Figs. 3-7**). The complete hard superellipse phase diagram can be summarized as a function of particle aspect ratio (r_y/r_x), shape parameter (n), and particle concentration (η) (**Fig.**

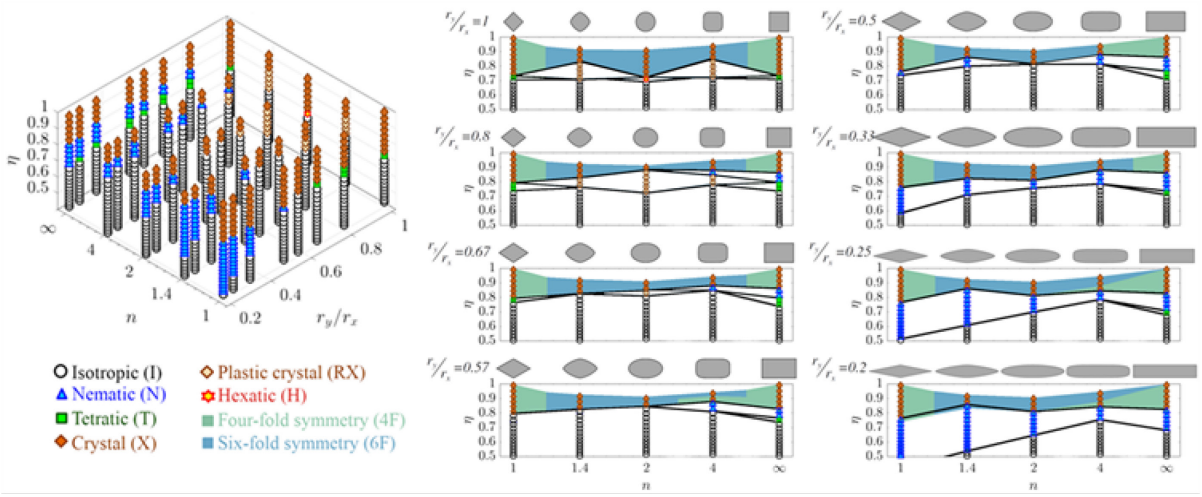

Fig. 8. Phase diagram for hard superellipses as a function of the aspect ratio (r_y/r_x), particle shape parameter (n), and area fraction (η). Phases indicated as: (○) isotropic, (▲) nematic, (■) tetratic, (◇) plastic crystal, or (◆) crystal, with symmetry indicated as (■) four-fold or (■) six-fold. Hexatic phase (✡) from large system size literature results.[11,12]

8). Given the results in **Figs. 3-7** show concentration dependent phases vs. aspect ratio for fixed shapes (n), we also show in **Fig. 8** alternative cross-sections of concentration dependent phases vs. shape (n) for fixed aspect ratio. In the following, we discuss general features and trends in the shape dependent phases (without exhaustively cataloging details).

We first consider global trends in the data. Although particle shape (n) is not a linear axis in the cross-sectional views (category plots on **Fig. 8** right), there is a degree of symmetry in several trends observed relative to the hard disk/ellipse case. Either decreasing sidewall curvature (n<2) or increasing corner curvature (n>2) produces crystals with 4-fold order, whereas shapes with $n \rightarrow 2$ yield crystals with 6-fold order. This leads to another effect already noted where stretched 4-fold bond orientational order continuously emerges within nematic phases prior to crystallization of 4-fold ordered crystals. In contrast, stretched 6-fold bond orientational order does not emerge in nematic phases for n=2 shapes, but rather abruptly increases with the onset of crystallization of 6-fold ordered crystals (as noted before, we do not attempt to resolve the hexatic phase and its boundaries based its known strong system size dependence[11,12]). Anisotropic particle sidewall and corner curvature appear to have a significant role in the structure of increasingly concentrated nematic phases leading to crystals with different symmetry. These findings are also consistent in the limit of isotropic particles, where squares have tetratic phases prior to forming square crystals and disks have hexatic phases before forming hexagonal crystals[20] (and all regular polygons with >5 sides go through a hexatic phase[21]).

Beyond the symmetry encountered within phases for different shapes, we also observe several trends for how shape influences types of phases and their concentration ranges. For example, nematic ordering is facilitated compared to a disordered liquid by sharp corners, flat sidewalls, and aspect ratio $r_y/r_x < 0.5$, which is seen in the largest concentration ranges for the most anisotropic rhombuses and rectangles. Rectangles over a limited aspect ratio range ($0.25 < r_y/r_x < 0.8$) also show a sort of biaxial nematic phase intermediate to tetratic and crystal phases, which is not observed for other shapes. In contrast to nematic phases, plastic crystal phases are facilitated for particle shapes with a combination of more rounded corners and sides ($1.4 < n < 4$) and lower aspect ratios ($r_y/r_x > 0.67$). Tetratic phases are facilitated by sharp corners ($n = 1, \infty$) in combination

with low aspect ratios ($r_y/r_x > 0.57$), although concentration ranges for tetratic phases are expected to strongly depend on system size (shown for squares[19,21]).

Finally, we note phases we do not observe in our study. We do not resolve a hexatic phase based on the small system sizes and limited resolution of phase boundaries in our work; this is unsurprising given the exceptionally large system sizes required to quantify the hexatic phase boundaries and transitions to liquid and solid phases.[11,12] We also do not observe a smectic phase for any shape, although they are known to form in non-equilibrium steady state quasi-2D vibrated granular systems (rice grains[51]) and cylindrical colloids (with rectangular cross sections) with induced dipolar potentials in AC electric fields.[52] This is consistent with other two-dimensional simulations of rods and rectangles that do not find smectic phases[42] (in contrast to three-dimensional systems of similar particle shapes[23]). Finally, we observed solid phases with either stretched 4-fold or 6-fold order, but did not observe (or investigate in detail the possibility of) previously reported solid phase variants for isotropic rounded squares[19,20,35] and cubes with depletion attraction and soft electrostatic repulsion.[24,26,27]

Conclusions

Our simulation results show how systematically varying particle sidewall and corner curvature together with particle aspect ratio produce different liquid crystal and crystal phases to provide design rules for two-dimensional particle assembly. Specifically, we investigated hard superellipse phases as a function of particle aspect ratio (r_y/r_x), sidewall and corner curvature via the superellipse parameter (n), and area fraction (η). Specific shapes investigated include disks, ellipses, squares, and rectangles, as well as, rounded squares, rounded rectangles, rounded rhombuses, and rhombuses. Using established methods to determine orientational order and several order parameters, as well as a novel stretched bond orientational order parameter, we show how phases, symmetry, and boundaries change systematically as a function of particle shape. We observe phases including isotropic, nematic, tetratic, plastic crystals, square crystals, and hexagonal crystals (including stretched variants).

Our results yield a number of new findings for how systematically varying particle shape influences the types of phases and their symmetry, the area fractions over which they are observed, and the emergence of bond orientational order within liquid crystal phases prior to crystallization. Our results also agree with benchmark shapes including hard disks, ellipses, squares, rounded squares, and rectangles. Many details of how shape parameters influence phases are cataloged within our results and discussion, but we summarize several global findings here in conclusion. Either flattening sidewalls or introducing increasingly sharp corners relative to the continuous curvature of the disk/ellipse case produces 4-fold order in crystal phases and within concentrated nematic phases. Nematic phases are present, and occur over greater concentration ranges, for particle shapes with flatter sidewalls, sharper corners, and increasing anisotropy above a threshold. In contrast, plastic phases are most likely for nearly isotropic particles with continuously varying curvature. Tetratic phases occur for a narrow range of conditions with flat sidewalls, sharp corners, and relatively low aspect ratios below a threshold. By demonstrating how particle sidewall and corner curvature together with anisotropy determine the existence and concentration range of phases, our findings provide broad understanding of how particle shape controls the presence of phases in two-dimensional particulate systems and enables the design of particle based microstructured materials.

Supporting Information

Supporting information is available containing simulation results for every particle system.

References

1. Glotzer, S.C. and M.J. Solomon, *Anisotropy of building blocks and their assembly into complex structures.* Nat Mater, 2007. **6**(7): p. 557-562.
2. Velev, O.D. and S. Gupta, *Materials Fabricated by Micro- and Nanoparticle Assembly – The Challenging Path from Science to Engineering.* Adv. Mat., 2009. **21**(19): p. 1897-1905.
3. Arpin, K.A., A. Mihi, H.T. Johnson, A.J. Baca, J.A. Rogers, J.A. Lewis, and P.V. Braun, *Multidimensional Architectures for Functional Optical Devices.* Adv. Mater., 2010. **22**(10): p. 1084-1101.
4. Wu, N., D. Lee, and A. Striolo, *Anisotropic Particle Assemblies*. 2018, Amsterdam: Elsevier.
5. Yu, K., T. Fan, S. Lou, and D. Zhang, *Biomimetic optical materials: Integration of nature's design for manipulation of light.* Progress in Materials Science, 2013. **58**(6): p. 825-873.
6. McDougal, A., B. Miller, M. Singh, and M. Kolle, *Biological growth and synthetic fabrication of structurally colored materials.* Journal of Optics, 2019. **21**(7): p. 073001.
7. Kosterlitz, J.M. and D.J. Thouless, *Ordering, metastability and phase transitions in two-dimensional systems.* Journal of Physics C: Solid State Physics, 1973. **6**(7): p. 1181-1203.
8. Halperin, B.I. and D.R. Nelson, *Theory of Two-Dimensional Melting.* Physical Review Letters, 1978. **41**(2): p. 121-124.
9. Nelson, D.R. and B.I. Halperin, *Dislocation-mediated melting in two dimensions.* Physical Review B, 1979. **19**(5): p. 2457-2484.
10. Young, A.P., *Melting and the vector Coulomb gas in two dimensions.* Phys. Rev. B, 1979. **19**(4): p. 1855-1866.
11. Bernard, E.P. and W. Krauth, *Two-Step Melting in Two Dimensions: First-Order Liquid-Hexatic Transition.* Physical Review Letters, 2011. **107**(15): p. 155704-155704.
12. Engel, M., J.A. Anderson, S.C. Glotzer, M. Isobe, E.P. Bernard, and W. Krauth, *Hard-disk equation of state: First-order liquid-hexatic transition in two dimensions with three simulation methods.* Physical Review E, 2013. **87**(4): p. 042134.
13. Cuesta, J.A. and D. Frenkel, *Monte Carlo simulation of two-dimensional hard ellipses.* Phys Rev A, 1990. **42**(4): p. 2126-2136.
14. Xu, W.-S., Y.-W. Li, Z.-Y. Sun, and L.-J. An, *Hard ellipses: Equation of state, structure, and self-diffusion.* The Journal of chemical physics, 2013. **139**(2): p. 024501.
15. Bautista-Carbajal, G. and G. Odriozola, *Phase diagram of two-dimensional hard ellipses.* The Journal of Chemical Physics, 2014. **140**(20): p. 204502.
16. Wojciechowski, K.W. and D. Frenkel, *Tetratic Phase In the Planar Hard Square System?* J. Compit. Methods Sci. Eng., 2004. **10**: p. 235.
17. Donev, A., J. Burton, F.H. Stillinger, and S. Torquato, *Tetratic order in the phase behavior of a hard-rectangle system.* Physical Review B, 2006. **73**(5).
18. Martinez-Raton, Y., E. Velasco, and L. Mederos, *Orientational ordering in hard rectangles: the role of three-body correlations.* J Chem Phys, 2006. **125**: p. 14501.
19. Avendaño, C. and F.A. Escobedo, *Phase behavior of rounded hard-squares.* Soft Matter, 2012. **8**(17): p. 4675.
20. Gurin, P., S. Varga, and G. Odriozola, *Three-step melting of hard superdisks in two dimensions.* Physical Review E, 2020. **102**(6): p. 062603.
21. Anderson, J.A., J. Antonaglia, J.A. Millan, M. Engel, and S.C. Glotzer, *Shape and Symmetry*

Determine Two-Dimensional Melting Transitions of Hard Regular Polygons. Physical Review X, 2017. **7**(2).
22. Harper, E.S., R.L. Marson, J.A. Anderson, G. van Anders, and S.C. Glotzer, *Shape allophiles improve entropic assembly.* Soft Matter, 2015. **11**(37): p. 7250-7256.
23. Bolhuis, P. and D. Frenkel, *Tracing the phase boundaries of hard spherocylinders.* The Journal of Chemical Physics, 1997. **106**(2): p. 666-687.
24. Zhao, K., R. Bruinsma, and T.G. Mason, *Entropic crystal-crystal transitions of Brownian squares.* Proc Natl Acad Sci U S A, 2011. **108**(7): p. 2684-7.
25. Zhao, K. and T.G. Mason, *Twinning of rhombic colloidal crystals.* J Am Chem Soc, 2012. **134**(43): p. 18125-31.
26. Rossi, L., V. Soni, D.J. Ashton, D.J. Pine, A.P. Philipse, P.M. Chaikin, M. Dijkstra, S. Sacanna, and W.T. Irvine, *Shape-sensitive crystallization in colloidal superball fluids.* Proc Natl Acad Sci U S A, 2015. **112**(17): p. 5286-90.
27. Meijer, J.-M., A. Pal, S. Ouhajji, H.N.W. Lekkerkerker, A.P. Philipse, and A.V. Petukhov, *Observation of solid–solid transitions in 3D crystals of colloidal superballs.* Nat. Comm., 2017. **8**(1): p. 14352.
28. Elbert, K.C., T. Vo, N.M. Krook, W. Zygmunt, J. Park, K.G. Yager, R.J. Composto, S.C. Glotzer, and C.B. Murray, *Dendrimer Ligand Directed Nanoplate Assembly.* ACS Nano, 2019.
29. Barker, J.A. and D. Henderson, *Perturbation Theory and Equation of State for Fluids. II. A Successful Theory of Liquids.* J. Chem. Phys., 1967. **47**(11): p. 4714-4721.
30. van der Beek, D. and H.N.W. Lekkerkerker, *Liquid Crystal Phases of Charged Colloidal Platelets.* Langmuir, 2004. **20**(20): p. 8582-8586.
31. Liu, B., T.H. Besseling, M. Hermes, A.F. Demirors, A. Imhof, and A. van Blaaderen, *Switching plastic crystals of colloidal rods with electric fields.* Nat Commun, 2014. **5**: p. 3092.
32. Barr, A.H., *Superquadrics and Angle-Preserving Transformations.* Computer Graphics and Applications, IEEE, 1981. **1**(1): p. 11-23.
33. Eppenga, R. and D. Frenkel, *Monte Carlo study of the isotropic and nematic phases of infinitely thin hard platelets.* Molecular Physics, 1984. **52**(6): p. 1303-1334.
34. Brumby, P.E., A.J. Haslam, E. de Miguel, and G. Jackson, *Subtleties in the calculation of the pressure and pressure tensor of anisotropic particles from volume-perturbation methods and the apparent asymmetry of the compressive and expansive contributions.* Molecular Physics, 2011. **109**(1): p. 169-189.
35. Jiao, Y., F.H. Stillinger, and S. Torquato, *Optimal packings of superdisks and the role of symmetry.* Phys Rev Lett, 2008. **100**(24): p. 245504.
36. Torres-Díaz, I. and M.A. Bevan, *General Potential for Anisotropic Colloid–Surface Interactions.* Langmuir, 2017. **33**(17): p. 4356-4365.
37. Torres-Díaz, I., B. Rupp, Y. Yang, and M.A. Bevan, *Energy landscapes for ellipsoids in non-uniform AC electric fields.* Soft Matter, 2018. **14**(6): p. 934-944.
38. Mickel, W., S.C. Kapfer, G.E. Schröder-Turk, and K. Mecke, *Shortcomings of the bond orientational order parameters for the analysis of disordered particulate matter.* The Journal of Chemical Physics, 2013. **138**(4): p. 044501.
39. Emiris, I.Z. and G.M. Tzoumas, *Exact and efficient evaluation of the InCircle predicate for parametric ellipses and smooth convex objects.* Computer-Aided Design, 2008. **40**(6): p. 691-700.
40. Lovrić, J., S. Kaliman, W. Barfuss, G.E. Schröder-Turk, and A.-S. Smith, *Geometric effects*

in random assemblies of ellipses. Soft Matter, 2019. **15**(42): p. 8566-8577.
41. Frenkel, D. and R. Eppenga, *Evidence for algebraic orientational order in a two-dimensional hard-core nematic.* Phys Rev A Gen Phys, 1985. **31**(3): p. 1776-1787.
42. Bates, M.A. and D. Frenkel, *Phase behavior of two-dimensional hard rod fluids.* The Journal of Chemical Physics, 2000. **112**(22): p. 10034-10041.
43. Geng, J. and J.V. Selinger, *Theory and simulation of two-dimensional nematic and tetratic phases.* Phys Rev E, 2009. **80**: p. 11707.
44. McMillan, W.L., *Simple Molecular Model for the SmecticAPhase of Liquid Crystals.* Physical Review A, 1971. **4**(3): p. 1238-1246.
45. Varga, S., P. Gurin, J.C. Armas-Pérez, and J. Quintana-H, *Nematic and smectic ordering in a system of two-dimensional hard zigzag particles.* The Journal of Chemical Physics, 2009. **131**(18): p. 184901.
46. Beltran-Villegas, D.J., R.M. Sehgal, D. Maroudas, D.M. Ford, and M.A. Bevan, *Colloidal Cluster Crystallization Dynamics.* J. Chem. Phys., 2012. **137**(13): p. 134901.
47. Yang, Y., R. Thyagarajan, D.M. Ford, and M.A. Bevan, *Dynamic colloidal assembly pathways via low dimensional models.* J. Chem. Phys., 2016. **144**(20): p. 204904.
48. Zhang, J., Y. Zhang, and M.A. Bevan, *Spatially Varying Colloidal Phase Behavior on Multi-Dimensional Energy Landscapes.* J. Chem. Phys., 2020. **152**: p. 054905.
49. Walsh, L. and N. Menon, *Ordering and dynamics of vibrated hard squares.* Journal of Statistical Mechanics: Theory and Experiment, 2016. **2016**(8): p. 083302.
50. Meijer, J.M., A. Pal, S. Ouhajji, H.N. Lekkerkerker, A.P. Philipse, and A.V. Petukhov, *Observation of solid-solid transitions in 3D crystals of colloidal superballs.* Nat Commun, 2017. **8**: p. 14352.
51. Narayan, V., N. Menon, and S. Ramaswamy, *Nonequilibrium steady states in a vibrated-rod monolayer: tetratic, nematic, and smectic correlations.* Journal of Statistical Mechanics: Theory and Experiment, 2006. **2006**(01): p. P01005-P01005.
52. Kuijk, A., T. Troppenz, L. Filion, A. Imhof, R. van Roij, M. Dijkstra, and A. van Blaaderen, *Effect of external electric fields on the phase behavior of colloidal silica rods.* Soft Matter, 2014. **10**(33): p. 6249-6255.

For Table of Contents Use Only

TOC text (1-2 sentences, <250 characters): Computer simulation results are reported for hard superellipse particle phases vs. particle aspect ratio and curvature. Findings indicate design rules for particle shapes that determine diverse two-dimensional liquid, liquid crystalline, and crystalline microstructures.

TOC graphic (8 cm (~3.14 in) wide x 4 cm (1.57 in) high, >600 dpi):